MATERIALS CHEMISTRY
FRONTIERS

RESEARCH ARTICLE

View Article Online
View Journal | View Issue

Cite this: *Mater. Chem. Front.*, 2021, **5**, 7993

Fast preparation of controllable nitrogen-atom-substituted graphyne film for use in field effect transistor devices†

Ze Yang,[a] Xin Ren,[b] Xiaodi Ma,[a] Yuwei Song,[a] Xiuli Hu,[a] Mingjia Zhang,[a] Yuan Li,[a] Chipeng Xie,[a] Xiaodong Li,[a] Jiazhu Li [b] and Changshui Huang *[a]

Received 18th May 2021,
Accepted 9th September 2021

DOI: 10.1039/d1qm00736j

rsc.li/frontiers-materials

It has been predicted that the introduction of heteroatoms into graphyne (GY) will be able to improve the properties of GY and increase its range of applications. However, it is difficult to synthesize GY, which is linked through only one acetylenic bond (–C≡C–) between any two adjacent benzene rings. Herein, we demonstrate an innovative interfacial synthetic method for rapid preparation of nitrogen-substituted GY (N-GY) films. Notably, as-prepared N-GY films that offer a determined morphology and well-established N atoms can be utilized as semiconductor films for field-effect transistor (FET) devices. With the increase in the number of N atoms in N-GY films, the carrier mobility of the prepared FET devices based on those N-GY films was increased. An average mobility of 9.8 $cm^2\ V^{-1}\ s^{-1}$ with a gate operating voltage lower than 5 V was measured for such rapidly prepared N-GY films, implying that interfacial synthesis can provide a facile avenue to obtain GY-based electronic materials. Thus, GY-based materials have the potential to become very promising candidates for incorporation into electronic devices.

Introduction

Due to their high conductivity, excellent electronic properties, and unique carbon skeleton, two dimensional (2D) carbon materials have been recognized as key components for the next generation of new electronic and optoelectronic devices.[1–4] Graphdiyne (GDY) is a relatively new substance composed of a large number of sp-hybridized carbon atoms,[5] and it is well-suited for applications in nanoelectronics because it delivers a natural band gap energy of 0.46 eV and a high theoretical carrier mobility of $5.41 \times 10^5\ cm^2\ V^{-1}\ s^{-1}$.[6–8] Since Prof. Li's pioneering work on the experimental preparation of GDY film on a copper (Cu) surface, the synthesis of GDY and its derivatives have been fervently developed and discussed.[9–21] Previously reported methods are based on the dehydrogenation coupling between the same monomers, which normally would be utilized for the synthesis of carbon materials with an even number of acetylenic linkages.[22–27] It is a considerable challenge to synthesize graphyne (GY), which is linked through only one acetylenic bond (–C≡C–) between any two adjacent benzene rings, and it is rarely reported.

To synthesize GY, great efforts and multitudinous attempts are still required. Interfacial synthesis, which can effectively control the morphology, has been applied to prepare 2D carbon materials. Many reports have been published describing the preparation of GDY and GDY derivatives through a liquid–liquid interface method.[28–30] In our previous reports, we developed an interface method to prepare a well-defined GY derivative (GYD) film composed of only one acetylenic bond between adjacent benzene rings, while the film morphology of such GYDs can be well controlled.[31] There are potential uses for these GYD films in electronic devices.

To obtain high performance of some electronic devices such as field-effect transistors (FETs), one of the crucial issues in maximizing the mobility is to control the film morphology of the sample.[32–34] According to many reports on heteroatom-doped carbon materials, adjusting the band gap of the GY by introducing heteroatoms such as N atoms can also be an effective method to improve the electronic performance.[35–37] The introduction of N atoms can change the charge distribution, adjust the band gap, facilitate electron transport, and increase the charge carrier mobility of the carbon materials.[38,39] N doping is still accompanied by some issues such as uncontrollable content and uncertain types, and

[a] *Qingdao Institute of Bioenergy and Bioprocess Technology, Chinese Academy of Sciences, No. 189 Songling Road, 266101, Qingdao, China. E-mail: huangcs@qibebt.ac.cn*
[b] *College of Chemistry and Chemical Engineering, Yantai University, Yantai 264005, China*

† Electronic supplementary information (ESI) available: Experimental details including the synthetic procedure, characterization, and device performance data. See DOI: 10.1039/d1qm00736j

therefore, it is difficult to verify the role that each type of N plays in the application process. Previously, we demonstrated the controllable introduction of N atoms to GDY through a 'bottom-up' synthetic strategy by adjusting the precursor molecules,[40,41] but those methods cannot be used for the synthesis of GYDs. Thus, there will be great significance in developing new methods to achieve atomically precise synthesis of N-substituted graphynes (N-GYs).

Herein, we developed a general and facile method for fast preparation of N-GY films using aza-aromatic alkynes and halogenated aza-aromatics through a liquid–liquid interface reaction. All these prepared N-GY films provide the same feature, which is the establishment of a single acetylenic linker between adjacent aza-aromatic rings. All the introduced N atoms are of the pyridinic type, of which the percentage is controlled by the number of N atoms in the aza-aromatic rings. The prepared N-GY sample not only appears as a continuous, uniform film in the macroscopic domain, but it also possesses a well-defined film-like structure at the microscopic and nanoscopic levels, which is mandatory for high-performance FET devices.

The novel carbon skeleton in the N-GY films can benefit the charge carrier mobility and the electrical conductivity of the films, while the introduced N atoms can tune the mobility and the performance of N-GY film-based FET devices. With the increase in the number of N atoms in N-GY films, the carrier mobility of the prepared FET devices based on those N-GY films was increased. The carrier mobility of a triazine-graphyne (TA-GY) film can reach 9.8 $cm^2 V^{-1} s^{-1}$, with a threshold voltage lower than 5 V, suggesting that these N-GY films have great potential for application in electronic and optical devices.

Results and discussion

Preparation and characterization of N-GY films

Importantly, increasing charge carrier mobility can achieve efficient current modulation and switching speeds in FET devices, while the morphology of the semiconductor film is one of the key factors that can improve the mobility.[32–34] For the purpose of quickly obtaining N-GY films with uniform morphology, we have developed a facile interface method that is performed at room temperature. As displayed in Scheme 1, 2,4,6-triethynyl-aza-aromatics were dissolved with dichloromethane (CH_2Cl_2) to form the organic phase. Then, pure water was slowly added along the wall of the crystallizing dish, constituting the aqueous phase. After dispersion, the aqueous system containing bis(triphenylphosphine) palladium(II) chloride, cuprous iodide (CuI), and 2,4,6-trichlorotriazine, was added dropwise to the water layer, which prevented the solution from directly dripping into the organic phase and maintained the stability of the two-phase interface. Catalysed by Pd/Cu, a cross-coupling reaction occurred at the liquid–liquid interface to form well-defined N-GY films. The methods used to synthesize pyridine-GY (PY-GY), pyrimidine-GY (PM-GY), and triazine-GY (TA-GY) are the same, with the only difference being the selected precursors. Photographs of the reaction at different stages are exhibited in Fig. S1 in the ESI.† The as-prepared uniform continuous films gradually become visible at the interface after reaction for 30 min. This liquid–liquid interface synthetic method is facile with excellent repeatability, and all the as-prepared N-GY films can be easily transferred to a silicon wafer for the preparation of FET devices.

Fig. 1a, e, and i exhibit the uniform macroscopic morphology of N-GY films observed on the liquid–liquid interface after reaction. After transfer to a silicon wafer, these N-GY films were examined by scanning electron microscopy (SEM), and images in Fig. 1b, f, and j reveal that they are flexible with a gauze-like membrane. Transmission electron microscopy (TEM) images (Fig. 1c, g and k) display the dispersed N-GY films as ultra-thin flat sheets at the nanoscopic level. These results show that the N-GY films appear to be uniform with a well-defined structure, which indicates that the interface synthesis can achieve satisfactory controllable film morphology. Elemental mapping

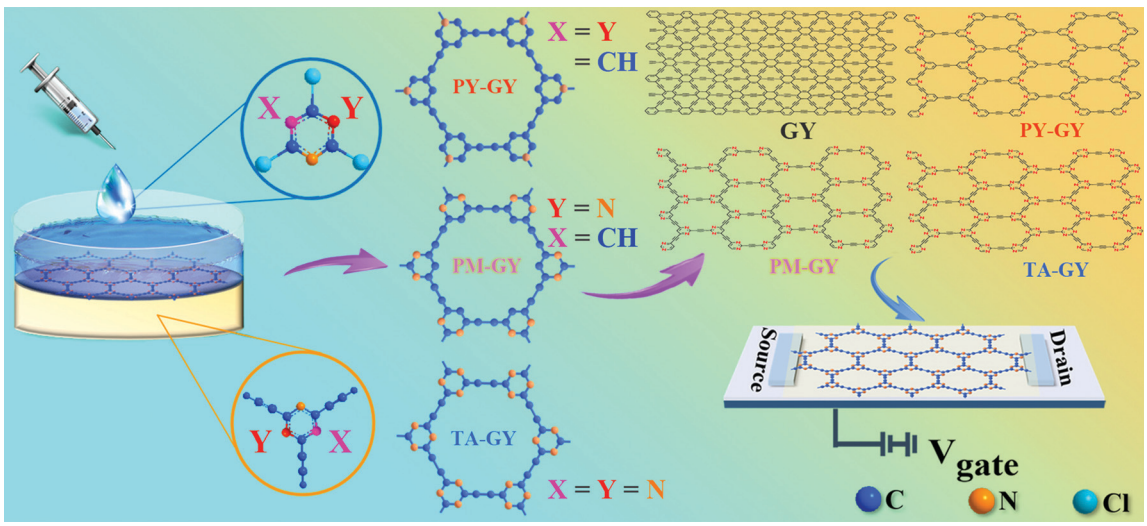

Scheme 1 Schematic illustration of the interface preparation process of N-GYs film and the related FET device.

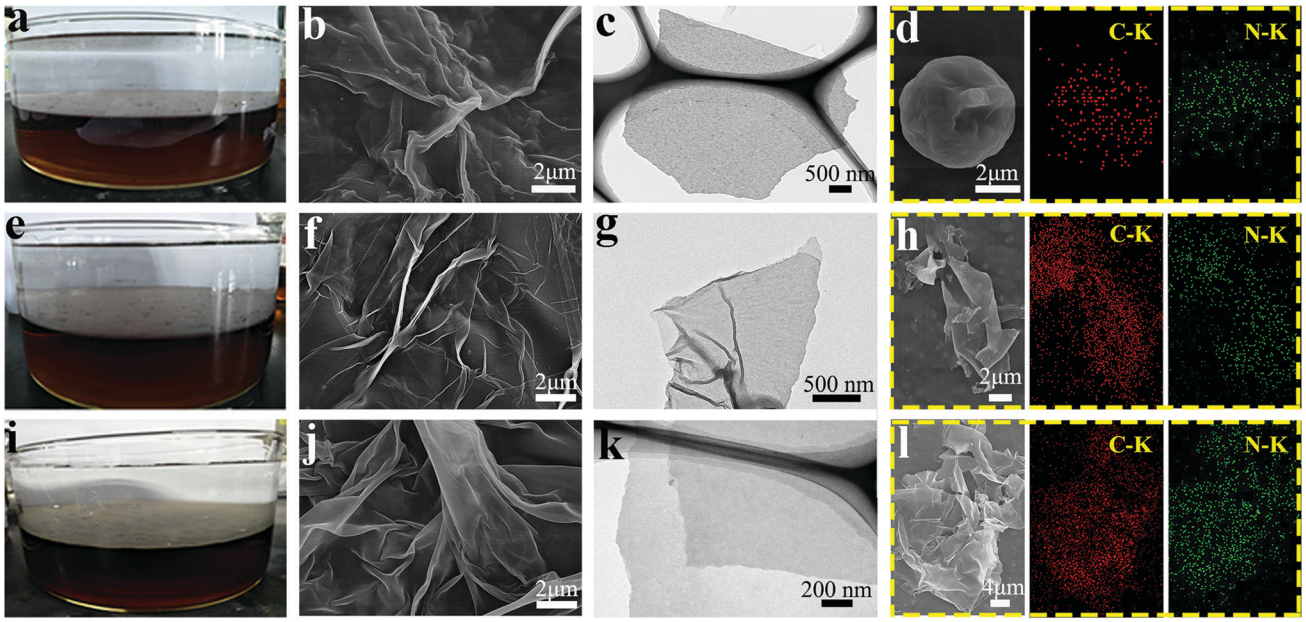

Fig. 1 The photographs of (a) PY-GY, (e) PM-GY and (i) TA-GY films on the liquid/liquid interface. SEM images of (b) PY-GY, (f) PM-GY and (j) TA-GY films. TEM images of (c) PY-GY, (g) PM-GY and (k) TA-GY films. EDX elemental mapping of C and N for (d) PY-GY, (h) PM-GY and (l) TA-GY films.

characterizations were performed to explore the element distribution in the N-GY films. As shown in Fig. 1d, h, and l, both carbon and N distribution domains are consistent with the morphology, suggesting that N atoms were uniformly introduced into the as-prepared N-GY films.

X-Ray photoelectron spectroscopy (XPS) was conducted to analyse the composition of these as-prepared N-GY films. In Fig. 2a, the C 1s peak of PY-GY can be well fitted and divided into five sub-peaks at 288.8 eV, 287.9 eV, 286.2 eV, 284.5 eV, and 285.1 eV, corresponding to C═O, C–O, N═C (sp^2), C–C (sp^2), and C–C (sp), respectively.[42–44] The C 1s peaks of PM-GY and TA-GY can also be assigned to C–C (sp^2), C–C (sp), C═N and C–C (sp), C═N, respectively. The details for the C 1s peaks of PM-GY and TA-GY are outlined in Fig. 2b and c. The XPS results show that the area ratio of C–C (sp^2), C═N (sp^2), and C–C (sp) of PY-GY and PM-GY are nearly 3 : 2 : 3 and 1 : 3 : 3, respectively, while the ratio of C═N and C–C (sp) in TA-GY is approximately 1 : 1, which demonstrates that the N/(C + N) atomic ratio of PY-GY, PM-GY, and TA-GY is 1.1/9, 2.0/9, and 3.0/9, respectively.

To further confirm the amounts of elements in the N-GY films, elemental analysis was performed. As listed in Table S1 of ESI,† the N mass percent was 11.86%, 22.90%, and 4.29% for PY-GY, PM-GY, and TA-GY, respectively. The atomic N/(C + N) ratios for PY-GY, PM-GY, and TA-GY are 0.99/9, 1.92/9, and 2.97/9, respectively, which closely coincide with the theoretical values of 1/9, 2/9, and 3/9. Therefore, both elemental analysis and the XPS results are in accord with the predesigned element composition and skeletal structure of these N-GY films. These accurate ratios of C/N also demonstrate that N atoms can be precisely introduced into GY according to the predesigned precursors. In addition, the N 1s peak of N-GY appearing at 399.9 eV (Fig. 2d), 399.8 eV (Fig. S2a, ESI†), and 399.7 eV (Fig. S2b, ESI†) can be ascribed to the pyridinic N in pyridine, pyrimidine, and triazine rings, implying that the introduced N is only one determined type in defined positions.[25,40,41,45]

The chemical composition of these N-GY films was also confirmed by Raman and Fourier transform infrared (FT-IR) spectroscopy. As displayed in Fig. 2e, the Raman results for the N-GY films exhibit typical absorption peaks composed of D and G bands. The D band at 1340–1360 cm^{-1} is related to the structural defects. The G peak at 1520–1600 cm^{-1} can be ascribed to the large amount of aromatic rings.[41,43] The peak at approximately 2200 cm^{-1} can be attributed to the stretching vibration of the acetylene bonds, demonstrating that these N-GY films are rich in acetylenic bonds.[43,46] In Fig. 2f, the FT-IR spectroscopy depicts a peak at 2170 cm^{-1}, which can be assigned to the stretching vibration of carbon–carbon triple bonds (–C≡C–). Furthermore, the peaks at 1350–1590 cm^{-1} can be attributed to the stretching vibration of the aromatic rings.[47,48]

These as-prepared N-GY films can be easily transferred. Fig. 2j shows a black TA-GY film transferred to a SiO_2/Si wafer with a size of 2 cm × 2 cm. We also characterized the N-GY films by UV-vis absorption spectroscopy to further understand the effect of the N-GY films on spectral absorption. The optical band gaps of the as-prepared N-GY films were measured to be 1.56 eV (Fig. S3a, ESI†), 1.58 eV (Fig. S3b, ESI†), and 1.42 eV (Fig. 2h) for PY-GY, PM-GY, and TA-GY, respectively, by following the relationship $\alpha \propto (h\nu - E_g)^{\frac{1}{2}}/h\nu$.[49] Those measured results are within the energy gap of the semiconductor, indicating that the prepared N-GY films are typical semiconductors. According to the current–voltage curves (Fig. 2i), the conductivities of the PY-GY, PM-GY, and TA-GY films are 2.0×10^{-2}, 2.1×10^{-2}, and 3.0×10^{-2} S m^{-1}, respectively, and they exhibit

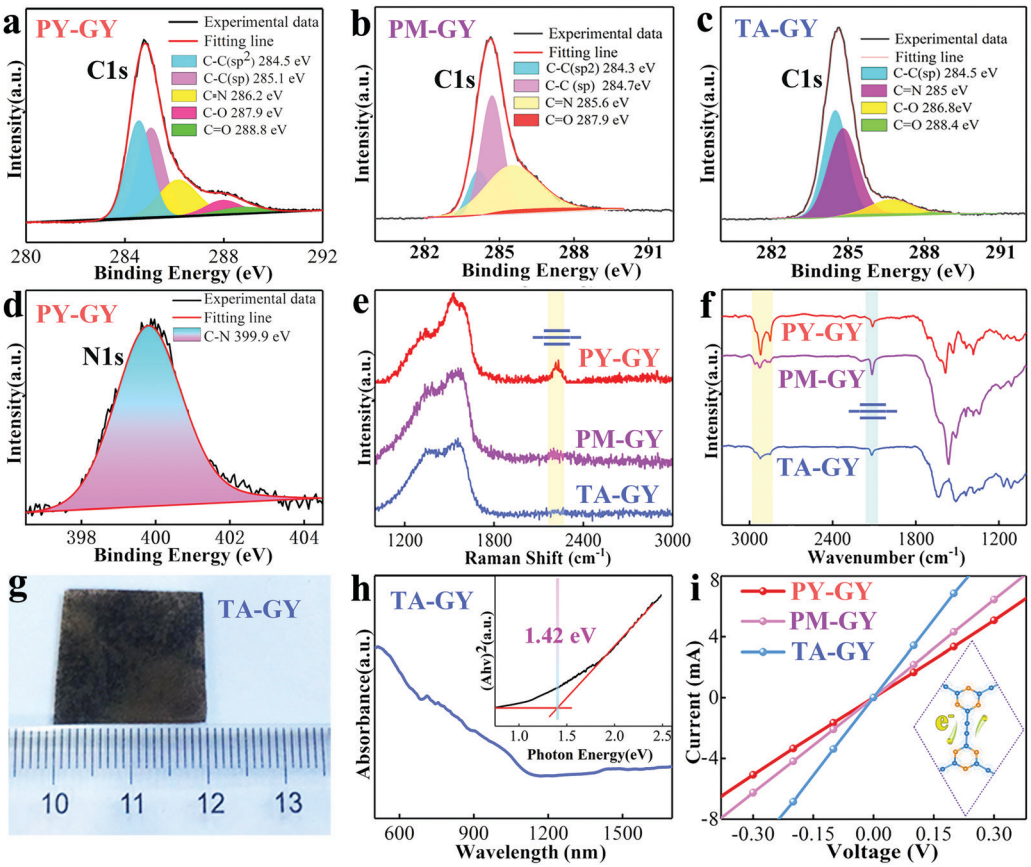

Fig. 2 Characterizations of N-GYs. XPS for C 1s of PY-GY (a), PM-GY (b) and TA-GY (c). (d) XPS for N 1s of PY-GY. (e) Raman, (f) FT-IR of N-GYs films. (g) The photograph and (h) UV-vis of the as-prepared TA-GY film. (i) *I*–*V* curves of N-GYs.

excellent semiconductor properties, thus ensuring brilliant development prospects for N-GY films in electrical and optical equipment.[50]

The XRD pattern of the as-prepared Si-DY (in Fig. S4, ESI†) exhibited a broad peak at 22–23°, which is similar to that of many reported carbon-based materials.[20,51] In addition, the band gap and conductivity are related to the quality of the prepared GY films, and thus, there will be a more accurate value of the conductivities by testing N-GY films obtained with high crystallinity or a single-layer as compared to those obtained *via* the fast preparation method.

DFT calculations for the N-GY films

To understand the influence of N atoms on the conductivity of the N-GY films, density functional theory (DFT) calculations were carried out. As displayed in Fig. 3a, d, and g, all atoms were in the same plane, implying that these N-GY films are well-defined 2D materials. Due to the effective adjustment of the reaction precursors, we were able to precisely control the site of the introduced N atoms, and also achieve multiple growth of the N atomic percentage. Furthermore, all the pyridinic N atoms are electron enrichment sites, and these can change the charge distribution, increase the electron cloud density, and improve the conductivity (see Fig. 3b, e and h).

As displayed in Fig. 3c, f, and i, the energy gaps for PY-GY, PM-GY, and TA-GY were 2.45, 2.32, and 2.30 eV, respectively, as obtained by density of states (DOS) calculation. To determine the influence of the layer number and defects in these as-prepared N-GY films, it was noted that the measured data were different from the calculated value. However, with the increase in the N percentage in the N-GY films, the variation trend of the theoretical value and actual value was consistent. The introduced pyridinic N atoms mainly contribute to the valence band and increase the total number of electrons and the electron cloud density, thereby reducing the band gap, and enhancing electrical conductivity.

Similar phenomena were also observed in PY-GY (Fig. 3c), PM-GY (Fig. 3f), and TA-GY (Fig. 3i). TA-GY offered the highest N percentage and narrowest band gap, which is consistent with the conductive performance shown in Fig. 2i. The measured conductivity and band gap of PY-GY (2.0×10^{-2} S m^{-1} and 1.56 eV) is similar to that of PM-GY (2.1×10^{-2} S m^{-1} and 1.58 eV), which may be related to the symmetry of the structural skeleton and the difference in the number of layers.[35,36]

To further explore the change in the band gap caused by the introduction of N, a single-layer hydrogen-substituted graphyne (HsGY, in Fig. 3j) and GY (Fig. 3m and Fig. S5, ESI†) simulation model were also used.[52,53] Because the valence electron of a carbon atom is one less than that of a N atom, the charge

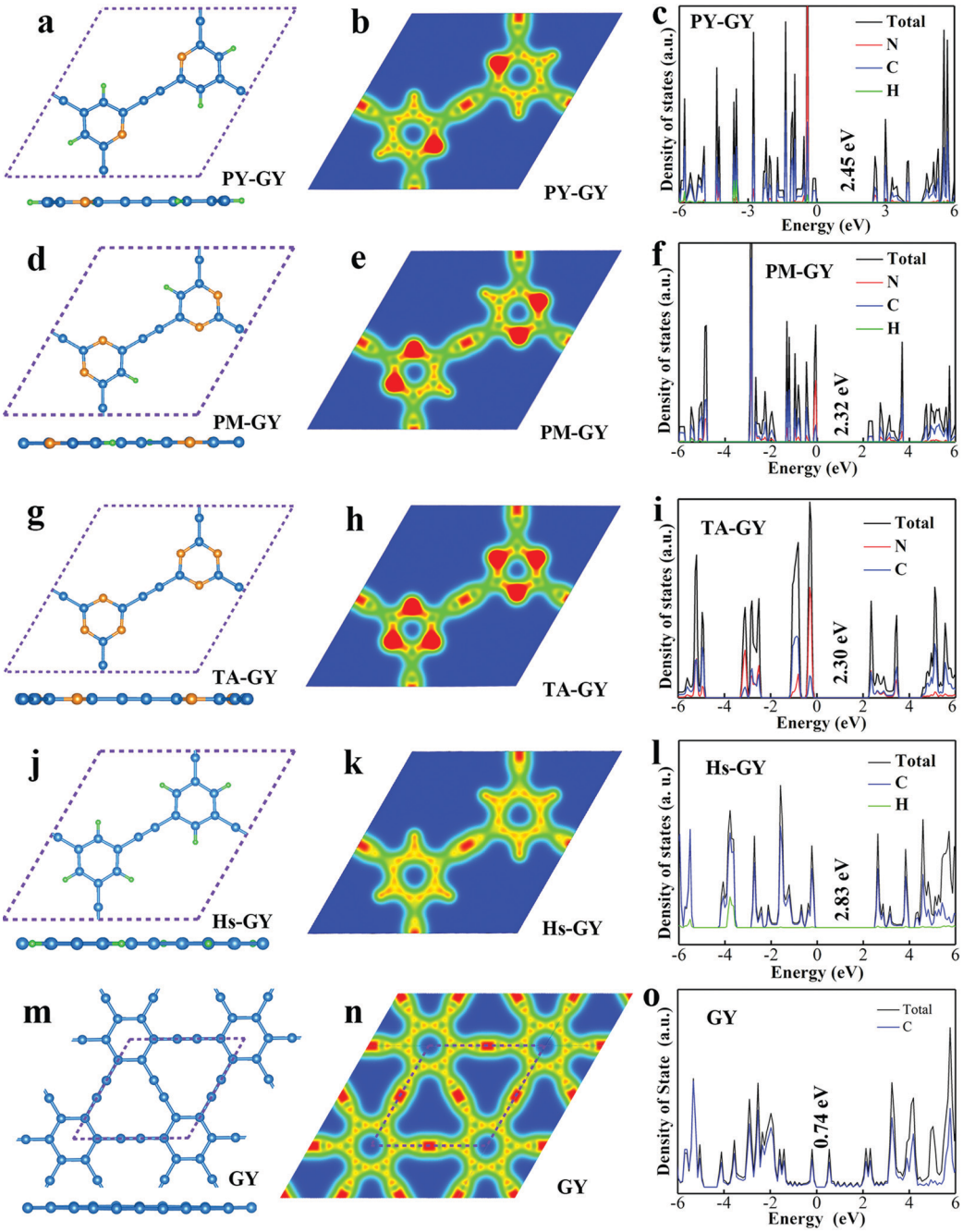

Fig. 3 (a) The optimized repeating unit of PY-GY from top and cross-section view. (b) Simulated charge density graphs and (c) the calculated DOS of PY-GY. (d) The optimized repeating unit of PM-GY from top and cross-section view. (e) Simulated charge density graphs and (f) the calculated DOS of PM-GY. (g) The optimized repeating unit of TA-GY from top and cross-section view. (h) Simulated charge density graphs and (i) the calculated DOS of TA-GY. (j) The optimized repeating unit of Hs-GY from top and cross-section view. (k) Simulated charge density graphs and (l) the calculated DOS of Hs-GY. (m) The optimized repeating unit of GY from top and cross-section view. (n) Simulated charge density graphs and (o) the calculated DOS of GY.

density of HsGY is lower than that of N-GY (Fig. 3k). The theoretical calculation results confirm that the band gap of Hs-GY without nitrogen atoms is larger than that of the N-GY films (Fig. 3l), which further proves that the introduction of N atoms can indeed increase the band gap. For the larger conjugated skeleton and the higher atomic and charge density in the single-layer GY model (Fig. 3n and Fig. S6, ESI†), the band gap was calculated with a lower value of 0.74 eV (Fig. 3o). All these results indicate that the perfect GY and N-GY can deliver great potential in electronic devices.

Application of N-GY films in FET

We further examined the performance of these rapidly prepared N-GY-film-based FET devices. As exhibited in Fig. 4a, N-GY films as semiconductors can be easily transferred to silicon wafers to fabricate FET devices. As shown in Fig. 4b–d,

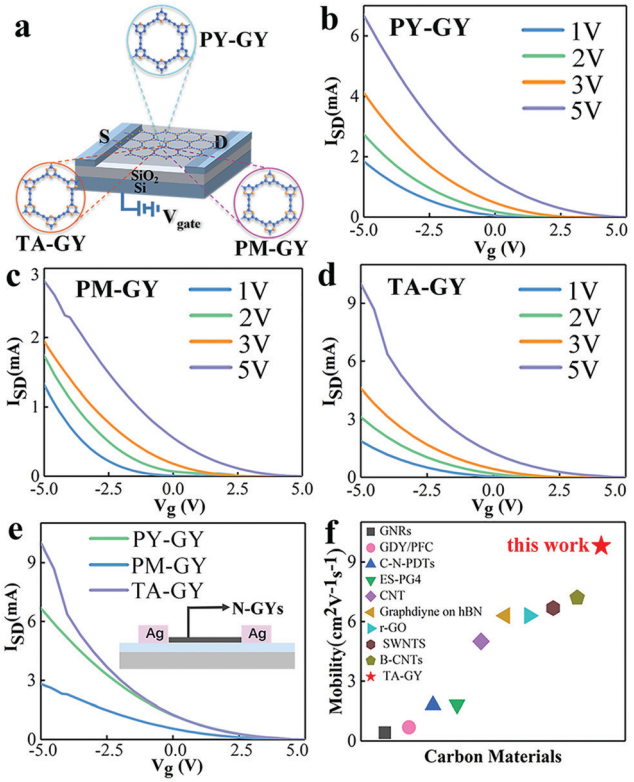

Fig. 4 (a) 3D schematic view of an N-GY-based transistor. The transfer I_{SD}–V_g curves for (b) PY-GY, (c) PM-GY, and (d) TA-GY. (e) The transfer I_{SD}–V_g curves for PY-GY, PM-GY, and TA-GY at the VDS of 5 V; the inset shows a schematic illustration of a N-GY-based FET device. (f) A comparison of carrier mobility with other carbon-based materials utilized in FET.

the transfer characteristics of these N-GY films were evaluated at V_{SD} (drain–source voltage) = 1, 2, 3, and 5 V, respectively. The transfer characteristics of N-GY films under different drain–source voltages deliver the same changing trend, and the threshold voltage is lower than 5 V. In addition, the switching ratio of TA-GY is higher than that of the other two materials, indicating that there is a stronger anti-interference ability of the TA-GY-based FET device. The transmission characteristics of N-GY films at V_{SD} = 5 V are depicted in Fig. 4e following the formula: $\mu = [dI/dV_g][L/(WC_gV_{SD})]$ (V_g: gate voltage, C_g: gate capacitance, L = 1 mm, W = 1 mm). The carrier mobility of PY-GY, PM-GY, and TA-GY films is calculated with the values of 6.26, 6.64, and 9.8 $cm^2\ V^{-1}\ s^{-1}$, respectively.

These results demonstrate that carrier mobility can be increased with introduced N atoms, which is in good agreement with the band gap and conductivity test results. Although the mobility of these rapidly prepared N-GY films is already high, there is still a large gap between the theoretical values for GY and N-GY, which indicates that there is still much room for improving the film quality of the as-prepared N-GY films. Furthermore, the development and preparation of defect-free or high-quality crystalline N-GY samples could be an important direction because it will increase mobility. Although these as-prepared N-GY films exhibit some deficiencies, the interfacial synthetic method is convenient and efficient for preparing N-GY films.

For additional comparison, HsGY was synthesized using this interface method, and the morphology and the FET performance were also characterized (Fig. S7 and S8, ESI†). As shown in Fig. S8 (ESI†), HsGY-based FET devices fabricated using the same procedure offer a mobility calculated at $7 \times 10^{-3}\ cm^2\ V^{-1}\ s^{-1}$. Obviously, the mobility of the as-prepared HsGY film is significantly lower than that of these rapidly prepared N-GY films, which further confirms that the introduced N atom is a key factor for improving the electronic and semiconductor properties. The N-GY film can be regarded as the 'fast channel' of charge transport in the conductive channel, which effectively reduces the length of the conductive path, thereby improving the output source-current.[54,55]

Additionally, we reviewed previous studies performed in the last few years that applied carbon materials in FET devices. A comprehensive comparison of the mobility in Fig. 4f proves that the as-prepared N-GY films are capable of a satisfactory performance, suggesting these N-GY films with determined morphology are promising semiconductor films for application in optoelectronic devices. More comparison references and related materials can be found in Table S2 of the ESI.†

Conclusions

In summary, we demonstrated a facile and efficient method for synthesis of N-GY films. Three well-defined N-GY films (PY-GY, PM-GY, and TA-GY) with determined N atoms were prepared using a liquid–liquid interface method. All three N-GY films delivered uniform film-like morphology not only in macroscopic domains, but also at the microscopic and nanoscopic level, indicating the potential application for FET devices.

These rapidly prepared N-GY films can be easily transferred to silicon wafers to assemble FET devices. With the increase in the number of N atoms in the N-GY films, the conductivity, band gap, and carrier mobility of the prepared FET devices based on those N-GY films were accordingly increased. The obtained carrier mobility can reach 9.8 $cm^2\ V^{-1}\ s^{-1}$, and the threshold operating voltage is lower than 5 V, which is more optimal than many other carbon materials, thus proving that the introduced N atoms can obviously affect the properties of GY-based film materials, and the GY-based materials can be potentially utilized in electronic and optical devices.

Experimental

Materials

Tetrahydrofuran (THF) was dried by distillation over sodium/benzophenone. Tetrabutylammonium fluoride (TBAF), zinc chloride ($ZnCl_2$), bis(triphenylphosphine) palladium(II) chloride ($PdCl_2(PPh_3)_2$), trimethylsilylacetylene ($(CH_3)_3SiC{\equiv}CH$), tetrakis-(triphenylphosphine)palladium ($Pd(PPh_3)_4$), 2,4,6-tribromopyridine, 2,4,6-trichloropyrimidine, 2,4,6-trichlorotriazine, and *n*-butyllithium (2.5 M in heptane) were purchased from J&K Scientific Ltd.

Morphological details were evaluated through transmission electron microscopy (TEM, HITACHI H-7650) and field emission scanning electron microscopy (FESEM, HITACHI S-4800). The chemical composition of the N-GY films was measured by X-ray photoelectron spectroscopy (XPS, VG Scientific ESCALab 220i-XL X-ray photoelectron spectrometer), Fourier transform infrared spectroscopy (FT-IR, Thermo-Fisher Nicolet iN10), and Raman spectroscopy (Thermo Scientific DXRxi, 532 nm).

Synthesis of the N-GY film

According to previously reported work, we successfully synthesized three reactive precursors, including 2,4,6-(trimethylsilyl) ethynylpyridine, 2,4,6-(trimethylsilyl)ethynylpyrimidine, and 2,4,6-(trimethylsilyl)ethynyltriazine. After deprotection, an 2,4,6-ethynyl-aza-aromatic (0.3 mmol) was dissolved in dichloromethane (200 mL) to form the organic phase. Then, pure water was slowly added to form the aqueous phase. 2,4,6-Trihalogenated aza-aromatics (2,4,6-tribromo-pyridine, or 2,4,6-trichloropyrimidine, or 2,4,6-trichlorotriazine) and bis(triphenylphosphine)palladium(II) chloride and CuI were ultrasonicated, dispersed in pure water, and then added dropwise to the water phase. Due to the difference in concentration and the Brownian motion, these two monomers regularly arrange and react at the interface, forming a uniform film.

Theoretical calculation

Density functional theory (DFT) predictions were performed based on our previous reports.[41] The functional proposed by Perdew, Burke, and Ernzerhof (PBE) within the generalized gradient approximation (GGA) was selected for determining the exchange–correlation potential, and the projector-augmented wave (PAW) method was used to generate the plane wave. The plane-wave cutoff energy of 500 eV and the *k*-point grid of $9 \times 9 \times 1$ were used for structural optimization and self-consistent field calculations. All the atomic positions were fully optimized until all components of the residual forces were smaller than 0.01 eV $Å^{-1}$, and the convergence threshold for self-consistent iteration was 10^{-6} eV. Slab models with a vacuum thickness of 20 Å were used to simulate the monolayer structure of PY-GY, PM-GY, and TA-GY. The density of states (DOS) of the three structures was calculated, and the charge density graph was simulated.

Electrochemical measurements

The prepared N-GY film was transferred to pure water for cleaning by a direct transfer method, and then transferred to the SiO_2 substrate. The silver source–drain electrode was evaporated for 15 min under the condition that the vacuum degree was lower than 10^{-5}, and then, the preparation of the electrode was completed. A Keithley 4200 semiconductor characterization system and Signatone probe were used for electrochemical testing.

Author contributions

C. H. and Z. Y. conceived the experiments and supervised the research. Z. Y., X. R., Y. S. and X. M. conducted the analysis and performed most of the experiments. Z. Y., X. L., Y. L., X. H., M. Z. and J. L. carried out the DFT calculations. Z. Y. and C. H. wrote the manuscript with assistance from all co-authors.

Conflicts of interest

There are no conflicts to declare.

Acknowledgements

This study was supported by the National Natural Science Foundation of China (21701182, 51822208, 21771187, 21790051, 21790050), the Taishan Scholars Program of Shandong Province (tsqn201812111), the Frontier Science Research Project (QYZDB-SSW-JSC052) of the Chinese Academy of Sciences, and the Institute Research Project (QIBEBT ZZBS 201809).

Notes and references

1 C. Huang, Y. Li, N. Wang, Y. Xue, Z. Zuo, H. Liu and Y. Li, Progress in Research into 2D Graphdiyne-Based Materials, *Chem. Rev.*, 2018, **118**, 7744–7803.
2 C. Biswas and Y. H. Lee, Graphene Versus Carbon Nanotubes in Electronic Devices, *Adv. Funct. Mater.*, 2011, **21**, 3806–3826.
3 Q. Tang, Z. Zhou and Z. Chen, Graphene-related nanomaterials: tuning properties by functionalization, *Nanoscale*, 2013, **5**, 4541–4583.
4 N. Wang, J. He, K. Wang, Y. Zhao, T. Jiu, C. Huang and Y. Li, Graphdiyne-Based Materials: Preparation and Application for Electrochemical Energy Storage, *Adv. Mater.*, 2019, **31**, 1803202.
5 K. Wang, X. Li, Y. Xie, J. He, Z. Yang, X. Shen, N. Wang and C. Huang, Artificial Thiophdiyne Ultrathin Layer as an Enhanced Solid Electrolyte Interphase for the Aluminum Foil of Dual-Ion Batteries, *ACS Appl. Mater. Interfaces*, 2019, **11**, 23990–23999.
6 J. Chen, J. Xi, D. Wang and Z. Shuai, Carrier Mobility in Graphyne Should Be Even Larger than That in Graphene: A Theoretical Prediction, *J. Phys. Chem. Lett.*, 2013, **4**, 1443–1448.
7 M. Q. Long, L. Tang, D. Wang, Y. L. Li and Z. G. Shuai, Electronic Structure and Carrier Mobility in Graphdiyne Sheet and Nanoribbons: Theoretical Predictions, *ACS Nano*, 2011, **5**, 2593–2600.
8 X. Gao, H. Liu, D. Wang and J. Zhang, Graphdiyne: synthesis, properties, and applications, *Chem. Soc. Rev.*, 2019, **48**, 908–936.
9 J. Zhou, J. Li, Z. Liu and J. Zhang, Exploring Approaches for the Synthesis of Few-Layered Graphdiyne, *Adv. Mater.*, 2019, **31**, 1803758.

10 H. Yu, Y. Xue and Y. Li, Graphdiyne and its Assembly Architectures: Synthesis, Functionalization, and Applications, *Adv. Mater.*, 2019, **31**, 1803101.
11 R. Sakamoto, N. Fukui, H. Maeda, R. Matsuoka, R. Toyoda and H. Nishihara, The Accelerating World of Graphdiynes, *Adv. Mater.*, 2019, **31**, 1804211.
12 H. Zheng, Y. Li, H. Liu, X. Yin and Y. Li, Construction of heterostructure materials toward functionality, *Chem. Soc. Rev.*, 2011, **40**, 4506–4524.
13 Y. Li, L. Xu, H. Liu and Y. Li, Graphdiyne and graphyne: from theoretical predictions to practical construction, *Chem. Soc. Rev.*, 2014, **43**, 2572–2586.
14 Y. Li, T. Liu, H. Liu, M. Z. Tian and Y. Li, Self-Assembly of Intramolecular Charge-Transfer Compounds into Functional Molecular Systems, *Acc. Chem. Res.*, 2014, **47**, 1186–1198.
15 M. Zhang, X. Wang, H. Sun, W. Ning and C. Huang, Enhanced paramagnetism of mesoscopic graphdiyne by doping with nitrogen, *Sci. Rep.*, 2017, **7**, 11535.
16 C. Huang, N. Wang, Y. Li, C. Li, J. Li, H. Liu and D. Zhu, A New Class of Conjugated Polymers Having Porphyrin, Poly(p-phenylenevinylene), and Fullerene Units for Efficient Electron Transfer, *Macromolecules*, 2006, **39**, 5319–5325.
17 M. Zhang, X. Wang, H. Sun, N. Wang, J. He, N. Wang, Y. Long, C. Huang and Y. Li, Induced Ferromagnetic Order of Graphdiyne Semiconductors by Introducing a Heteroatom, *ACS Cent. Sci.*, 2020, **6**, 950–958.
18 T. Lu, J. He, R. Li, K. Wang, Z. Yang, X. Shen, Y. Li, J. Xiao and C. Huang, Adjusting the interface structure of graphdiyne by H and F co-doping for enhanced capacity and stability in Li-ion battery, *Energy Storage Mater.*, 2020, **29**, 131–139.
19 J. He, K. Bao, W. Cui, J. Yu, C. Huang, X. Shen, Z. Cui and N. Wang, Construction of Large-Area Uniform Graphdiyne Film for High-Performance Lithium-Ion Batteries, *Chem. – Eur. J.*, 2018, **24**, 1187–1192.
20 Q. Lv, N. Wang, W. Si, Z. Hou, X. Li, X. Wang, F. Zhao, Z. Yang, Y. Zhang and C. Huang, Pyridinic nitrogen exclusively doped carbon materials as efficient oxygen reduction electrocatalysts for Zn–air batteries, *Appl. Catal., B*, 2020, **261**, 118234.
21 C. Xie, X. Hu, Z. Guan, X. Li, F. Zhao, Y. Song, Y. Li, X. Li, N. Wang and C. Huang, Tuning the Properties of Graphdiyne by Introducing Electron-Withdrawing/Donating Groups, *Angew. Chem., Int. Ed.*, 2020, **59**, 13542–13546.
22 L. Hui, Y. Xue, H. Yu, Y. Liu, Y. Fang, C. Xing, B. Huang and Y. Li, Highly Efficient and Selective Generation of Ammonia and Hydrogen on a Graphdiyne-Based Catalyst, *J. Am. Chem. Soc.*, 2019, **141**, 10677–10683.
23 L. Hui, Y. Xue, B. Huang, H. Yu, C. Zhang, D. Zhang, D. Jia, Y. Zhao, Y. Li, H. Liu and Y. Li, Overall water splitting by graphdiyne-exfoliated and -sandwiched layered double-hydroxide nanosheet arrays, *Nat. Commun.*, 2018, **9**, 5309.
24 Y. Xue, B. Huang, Y. Yi, Y. Guo, Z. Zuo, Y. Li, Z. Jia, H. Liu and Y. Li, Anchoring zero valence single atoms of nickel and iron on graphdiyne for hydrogen evolution, *Nat. Commun.*, 2018, **9**, 1460.
25 Z. Yang, Y. Song, X. Ren, C. Zhang, X. Hu, X. Li, K. Wang, J. Li and C. Huang, A universal way to prepare graphyne derivatives with variable band gap and lithium storage properties, *Carbon*, 2021, **182**, 413–421.
26 W. Si, Z. Yang, X. Hu, Q. Lv, X. Li, F. Zhao, J. He and C. Huang, Preparation of zero valence Pd nanoparticles with ultra-efficient electrocatalytic activity for ORR, *J. Mater. Chem. A*, 2021, **9**, 14507–14514.
27 Z. Yang, Y. Song, C. Zhang, J. He, X. Li, X. Wang, N. Wang, Y. Li and C. Huang, Porous 3D Silicon-Diamondyne Blooms Excellent Storage and Diffusion Properties for Li, Na, and K Ions, *Adv. Energy Mater.*, 2021, 2101197.
28 R. Matsuoka, R. Sakamoto, K. Hoshiko, S. Sasaki, H. Masunaga, K. Nagashio and H. Nishihara, Crystalline Graphdiyne Nanosheets Produced at a Gas/Liquid or Liquid/Liquid Interface, *J. Am. Chem. Soc.*, 2017, **139**, 3145–3152.
29 X. Kan, Y. Ban, C. Wu, Q. Pan, H. Liu, J. Song, Z. Zuo, Z. Li and Y. Zhao, Interfacial Synthesis of Conjugated Two-Dimensional N-Graphdiyne, *ACS Appl. Mater. Interfaces*, 2018, **10**, 53–58.
30 Q. Pan, H. Liu, Y. Zhao, S. Chen, B. Xue, X. Kan, X. Huang, J. Liu and Z. Li, Preparation of N-Graphdiyne Nanosheets at Liquid/Liquid Interface for Photocatalytic NADH Regeneration, *ACS Appl. Mater. Interfaces*, 2019, **11**, 2740–2744.
31 Y. Song, X. Li, Z. Yang, J. Wang, C. Liu, C. Xie, H. Wang and C. Huang, A facile liquid/liquid interface method to synthesize graphyne analogs, *Chem. Commun.*, 2019, **55**, 6571–6574.
32 T. Kyu, An, S.-M. Park, S. Nam, J. Hwang, S.-J. Yoo, M.-J. Lee, W. Min Yun, J. Jang, H. Cha, J. Hwang, S. Park, J. Kim, D. Sung Chung, Y.-H. Kim, S.-K. Kwon and C. Eon Park, Thin Film Morphology Control *via* a Mixed Solvent System for High-Performance Organic Thin Film Transistors, *Sci. Adv. Mater.*, 2013, **5**, 1323–1327.
33 W. Shao, H. Dong, L. Jiang and W. Hu, Morphology control for high performance organic thin film transistors, *Chem. Sci.*, 2011, **2**, 590–600.
34 H. N. Tsao and K. Mullen, Improving polymer transistor performance via morphology control, *Chem. Soc. Rev.*, 2010, **39**, 2372–2386.
35 X. Dai and D. Ge, Numerical investigation on the field emission properties of N-doped graphdiyne-C_{60} nanostructures, *AIP. Adv.*, 2018, **8**, 015320.
36 Q. Lv, W. Si, J. He, L. Sun, C. Zhang, N. Wang, Z. Yang, X. Li, X. Wang, W. Deng, Y. Long, C. Huang and Y. Li, Selectively nitrogen-doped carbon materials as superior metal-free catalysts for oxygen reduction, *Nat. Commun.*, 2018, **9**, 3376.
37 Q. Lv, W. Si, Z. Yang, N. Wang, Z. Tu, Y. Yi, C. Huang, L. Jiang, M. Zhang, J. He and Y. Long, Nitrogen-Doped Porous Graphdiyne: A Highly Efficient Metal-Free Electrocatalyst for Oxygen Reduction Reaction, *ACS Appl. Mater. Interfaces*, 2017, **9**, 29744–29752.
38 A. Mohajeri and A. Shahsavar, Tailoring the optoelectronic properties of graphyne and graphdiyne: nitrogen/sulfur dual doping versus oxygen containing functional groups, *J. Mater. Sci.*, 2017, **52**, 5366–5379.

39 R. Sakamoto, R. Shiotsuki, K. Wada, N. Fukui, H. Maeda, J. Komeda, R. Sekine, K. Harano and H. Nishihara, A pyrazine-incorporated graphdiyne nanofilm as a metal-free electrocatalyst for the hydrogen evolution reaction, *J. Mater. Chem. A*, 2018, **6**, 22189–22194.

40 Z. Yang, R. Liu, N. Wang, J. He, K. Wang, X. Li, X. Shen, X. Wang, Q. Lv, M. Zhang, J. Luo, T. Jiu, Z. Hou and C. Huang, Triazine-graphdiyne: A new nitrogen-carbonous material and its application as an advanced rechargeable battery anode, *Carbon*, 2018, **137**, 442–450.

41 Z. Yang, X. Shen, N. Wang, J. He, X. Li, X. Wang, Z. Hou, K. Wang, J. Gao, T. Jiu and C. Huang, Graphdiyne Containing Atomically Precise N Atoms for Efficient Anchoring of Lithium Ion, *ACS Appl. Mater. Interfaces*, 2019, **11**, 2608–2617.

42 R. J. Liu, H. B. Liu, Y. L. Li, Y. P. Yi, X. K. Shang, S. S. Zhang, X. L. Yu, S. J. Zhang, H. B. Cao and G. J. Zhang, Nitrogen-doped graphdiyne as a metal-free catalyst for high-performance oxygen reduction reactions, *Nanoscale*, 2014, **6**, 11336–11343.

43 G. X. Li, Y. L. Li, H. B. Liu, Y. B. Guo, Y. J. Li and D. B. Zhu, Architecture of graphdiyne nanoscale films, *Chem. Commun.*, 2010, **46**, 3256–3258.

44 J. Y. Zhou, X. Gao, R. Liu, Z. Q. Xie, J. Yang, S. Q. Zhang, G. M. Zhang, H. B. Liu, Y. L. Li, J. Zhang and Z. F. Liu, Synthesis of Graphdiyne Nanowalls Using Acetylenic Coupling Reaction, *J. Am. Chem. Soc.*, 2015, **137**, 7596–7599.

45 W. T. Wu, J. Q. Zhang, W. Y. Fan, Z. T. Li, L. Z. Wang, X. M. Li, Y. Wang, R. Q. Wang, J. T. Zheng, M. B. Wu and H. B. Zeng, Remedying Defects in Carbon Nitride To Improve both Photooxidation and H-2 Generation Efficiencies, *ACS Catal.*, 2016, **6**, 3365–3371.

46 C. S. Huang, S. L. Zhang, H. B. Liu, Y. J. Li, G. T. Cui and Y. L. Li, Graphdiyne for high capacity and long-life lithium storage, *Nano Energy*, 2015, **11**, 481–489.

47 B. Jurgens, E. Irran, J. Senker, P. Kroll, H. Muller and W. Schnick, Melem (2,5,8-triamino-tri-*s*-triazine), an important intermediate during condensation of melamine rings to graphitic carbon nitride: Synthesis, structure determination by X-ray powder diffractometry, solid-state NMR, and theoretical studies, *J. Am. Chem. Soc.*, 2003, **125**, 10288–10300.

48 P. Kuhn, M. Antonietti and A. Thomas, Porous, covalent triazine-based frameworks prepared by ionothermal synthesis, *Angew. Chem., Int. Ed.*, 2008, **47**, 3450–3453.

49 T. Yu, B. Lim and Y. N. Xia, Aqueous-Phase Synthesis of Single-Crystal Ceria Nanosheets, *Angew. Chem., Int. Ed.*, 2010, **49**, 4484–4487.

50 Y. H. Jing, G. X. Wu, L. C. Guo, Y. Sun and J. Shen, Electronic transport properties of graphyne and its family, *Comput. Mater. Sci.*, 2013, **78**, 22–28.

51 J. He, N. Wang, Z. Cui, H. Du, L. Fu, C. Huang, Z. Yang, X. Shen, Y. Yi, Z. Tu and Y. Li, Hydrogen substituted graphdiyne as carbon-rich flexible electrode for lithium and sodium ion batteries, *Nat. Commun.*, 2017, **8**, 1172.

52 X. Ren, X. Li, Z. Yang, X. Wang, J. He, K. Wang, J. Yin, J. Li and C. Huang, Tailoring Acetylenic Bonds in Graphdiyne for Advanced Lithium Storage, *ACS Sustainable Chem. Eng.*, 2020, **8**, 2614–2621.

53 Z. Yang, C. F. Zhang, Z. F. Hou, X. Wang, J. J. He, X. D. Li, Y. W. Song, N. Wang, K. Wang, H. L. Wang and C. S. Huang, Porous hydrogen substituted graphyne for high capacity and ultra-stable sodium ion storage, *J. Mater. Chem. A*, 2019, **7**, 11186–11194.

54 Y. Li, M. Zhang, X. Hu, L. Yu, X. Fan, C. Huang and Y. Li, Graphdiyne-based flexible respiration sensors for monitoring human health, *Nano Today*, 2021, **39**, 101214.

55 X. Qian, H. Liu, C. Huang, S. Chen, L. Zhang, Y. Li, J. Wang and Y. Li, Self-catalyzed growth of large-area nanofilms of two-dimensional carbon, *Sci. Rep.*, 2015, **5**, 7756.